Inorganic Chemistry

Article

pubs.acs.org/IC

Electronic and Spectroscopic Properties of Avobenzone Derivatives Attached to Ditungsten Quadruple Bonds

Malcolm H. Chisholm,*[,†] Terry L. Gustafson,*[,†] William T. Kender,[†] Thomas F. Spilker,[‡] and Philip J. Young[†]

[†]Department of Chemistry and Biochemistry, The Ohio State University, 100 West 18th Avenue, Columbus, Ohio 43210, United States

[‡]Department of Macromolecular Science and Engineering, Case Western Reserve University, 2080 Adelbert Road, Cleveland, Ohio 44106, United States

Supporting Information

ABSTRACT: From the reactions between $W_2(T^iPB)_4$, where T^iPB is 2,4,6-triisopropylbenzoate, and 2 equiv of acid, 4-formylbenzoic acid, HBzald, 4-(3-oxo-3-phenylpropanoyl)benzoic acid, HAvo, or 4-(2,2-difluoro-6-phenyl-2*H*-1λ^3,3,2λ^4-dioxaborinin-4-yl)benzoic acid, $HAvoBF_2$, three new compounds $W_2(T^iPB)_2(Bzald)_2$, **I**, $W_2(T^iPB)_2(Avo)_2$, **II**, and $W_2(T^iPB)_2(AvoBF_2)_2$, **III**, have been prepared. As solid compounds **I** and **II** are blue while compound **III** is green. Characterization of these compounds has been carried out by means of ^{1}H NMR, MALDI-TOF MS, steady-state absorption and emission spectroscopies, and femtosecond and nanosecond transient absorption and time-resolved infrared spectroscopies. Compounds **I** and **II** have strong metal to ligand charge transfer, MLCT, transitions in the visible region of their spectra while compound **III** exhibits MLCT absorption in the near-infrared (λ_{max} = 1017 nm). All three have S_1 states that have corresponding lifetimes of ∼3−30 ps and are ^{1}MLCT in character. The triplet states are ^{3}MLCT with lifetimes in the range 3−10 ns. Density functional theory and time-dependent density functional theory were employed to perform electronic structure calculations in order to aid in the interpretation of these data. The spectroscopic properties of **I** and **II** are similar while the planarity of the ligand in **III** greatly lowers the energy of the MLCT state. The W_2 unit enables direct observation of intersystem crossing from the ^{1}MLCT state to ^{3}MLCT state via the use of ultrafast spectroscopy.

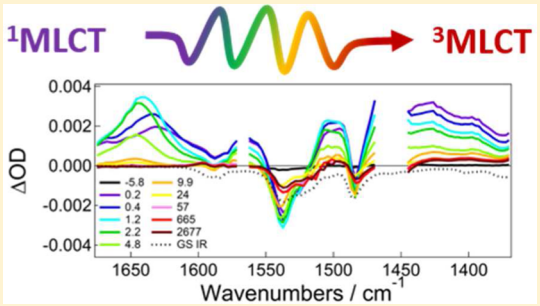

INTRODUCTION

Avobenzone is a molecular UVA filter found in many sunscreens. Upon absorbing UV light, it photoisomerizes from the enol form to the keto form.[1,2] The ground state of the latter form can be excited to access the T_1 state which undergoes photodecomposition.[3] This process is summarized in Scheme 1.[4]

Scheme 1. Summary of the Processes Occurring with the Avobenzone Molecule upon Photoexcitation

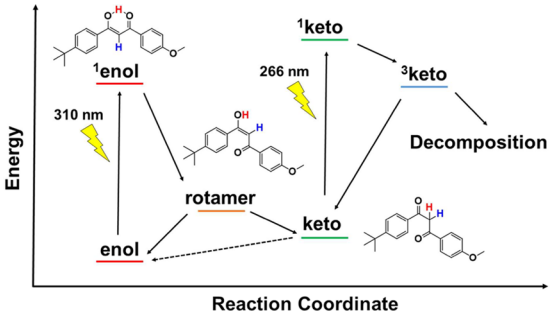

In previous work we have synthesized carboxylate derivatives of the avobenzone molecule and subsequently attached them to Mo_2-quadruply bonded units. These were studied due to their relatively long-lived ^{1}MLCT states, τ_1 = 5−15 ps, prior to converting to ^{3} $Mo_2\delta\delta^*$ states that have lifetimes of 7−64 μs. The molecules are of the type *trans*-$Mo_2(T^iPB)_2L_2$ complexes, where L = Bzald, Avo, and $AvoBF_2$.[5] See Chart 1.

In these compounds we have shown that the planar L−Mo_2−L unit is favored due to extensive Lπ−$Mo_2\delta$−Lπ conjugation. The structures of several compounds of this type have been determined,[6] and in previous work we discovered that this was also the case for $Mo_2(T^iPB)_2(Bzald)_2$.[5] See Figure 1.

In this earlier work we showed that UV−vis irradiation did not involve the enol to keto transformation, but rather internal conversion transformed the LL$\pi\pi^*$ transition to the lower energy ^{1}MLCT state. The latter lasted τ_1 = 13 ps and underwent conversion to the ^{3} $Mo_2\delta\delta^*$ state. This deactivation process was shown to prevent the light activated decomposition of the $Mo_2(T^iPB)_2(Avo)_2$ molecule as compared to that of the free ligand HAvo under the same photolysis conditions.[5]

Received: June 1, 2015
Published: September 21, 2015

DOI: 10.1021/acs.inorgchem.5b01221
Inorg. Chem. 2015, 54, 9438−9446

Chart 1. Structures, Abbreviations, and Formal Names Used in This Paper for the Three Ligands

Structure	Abbreviation	Formal Name
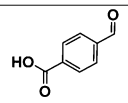	HBzald	4-formylbenzoic acid
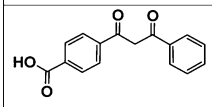	HAvo	4-(3-oxo-3-phenylpropanoyl)benzoic acid
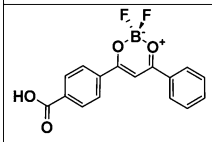	$HAvoBF_2$	4-(2,2-difluoro-6-phenyl-2*H*-1λ³,3,2λ⁴-dioxaborinin-4-yl)benzoic acid

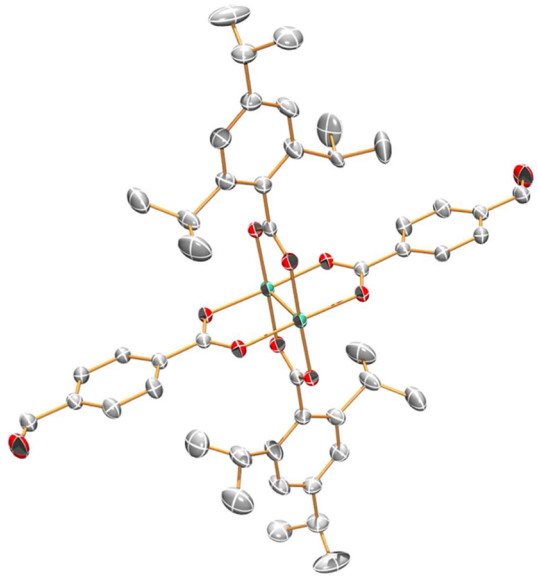

Figure 1. Molecular structure of $Mo_2Bzald_2T^iPB_2$ drawn at 50% probability. Colors as assigned as follows: blue = molybdenum, scarlet = oxygen, and gray = carbon. Hydrogens, solvent, and disorder omitted for clarity. Adapted from ref 5.

Although these compounds are air sensitive, it is not unreasonable to suggest that the incorporation of a metal could similarly deactivate this photoresponse.

As a continuation of the study of these ligands, here we describe our attachment of the same ligands to the W_2 center as in *trans*-$W_2(T^iPB)_2L_2$, where L= Bzald, **I**, Avo, **II**, and $AvoBF_2$, **III**, together with their physical properties. In particular we note that these compounds have lower energy ^{1}MLCT states, and that the triplet states are ^{3}MLCT in character as opposed to ^{3} $M_2\delta\delta^*$. Since both the S_1 and T_1 states extend over the ligand, we can now compare the properties of the charge localization in both singlet and triplet states using ultrafast time-resolved infrared spectroscopy.

RESULTS AND DISCUSSION

Syntheses. The new compounds **I**, **II**, and **III** were synthesized by the reaction shown in eq 1 below, where $W_2T^iPB_4$ was stirred with 2 equiv of the respective carboxylic acid. The reactions were carried out in toluene for 3 days, and some of the products were formed as powders. A reduction in the volume of solution was attained by evaporation of the solvent with a dynamic vacuum resulting in greater product formation. The resulting solids were collected by filtration and then washed with methanol, toluene, and hexanes. The MeOH and toluene solutions contained unreacted materials, and any excess T^iPBH was removed by the hexanes wash. Compounds **I** and **II** are deep blue, and compound **III** is deep green as a solid and pale yellow-green in dilute solutions. All three compounds are soluble in THF, though to a lesser extent than the Mo_2 analogues, and have been manipulated under inert atmosphere with dry, deoxygenated solvents as they are air and moisture sensitive.

$$W_2(T^iPB)_4 + 2LH \xrightarrow[RT,3days]{toluene} \textit{trans}\text{-}W_2(T^iPB)_2L_2 + 2T^iPBH \quad (1)$$

The compounds were characterized by ^{1}H NMR spectra; these are shown in the Supporting Information, SI, Figures S1–S3, and data are given in the Experimental Section. The ground state IR spectra were recorded and are noted as traces in the time-resolved infrared spectra. The high resolution MALDI-TOF-MS spectra give discrete molecular ions. The molecular ion of III^+ is shown in Figure 2. The spectra of I^+ and II^+ are given in Figures S4 and S5.

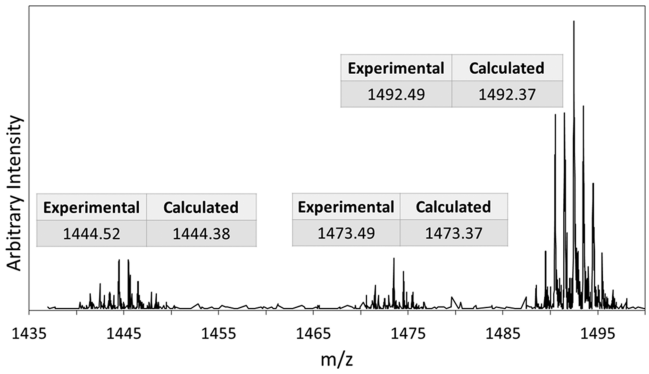

Figure 2. III^+ ion from the MALDI-TOF-MS, showing the fragmentation products $(III\text{-}F)^+$ at 1473.49 and $(III\text{-}BF_2) + H^+$ at 1444.52.

The spectra recorded for III^+ were notably weaker than the other spectra. In addition to the molecular ion peak, III^+, there are two loss products that can be observed: the formation of $(III\text{-}F)^+$ and a smaller quantity of $(III\text{-}BF_2) + H^+$. These peaks are due to the fragmentation of the oxygen boron bonds in addition to proton absorption from the matrix. The assignment of these peaks is confirmed by the ^{1}H NMR for compound **III** which does not contain any evidence of the fragmentation products prior to analysis by MALDI-TOF MS.

Electronic Structure Calculations. In order to assist in the determination of the spectral data, we performed density functional theory, DFT, calculations on the model compounds $W_2(O_2CH)_2L_2$, where L = Bzald, **I**′, Avo, **II**′, and $AvoBF_2$, **III**′. In these calculations, the T^iPB ligand is replaced with formate. This minimizes the consumption of computational resources, and since the T^iPB ligands are rotated ∼80–90° from the CO_2 moiety, this replacement of the ligands does not greatly affect the electronic structure.[7] Additionally, time-dependent DFT calculations were performed in order to obtain the simulated UV–vis spectra. Calculations on the anions $[I]^-$, $[II]^-$, and $[III]^-$, where the negative charge is localized on the ligands

DOI: 10.1021/acs.inorgchem.5b01221
Inorg. Chem. 2015, 54, 9438–9446

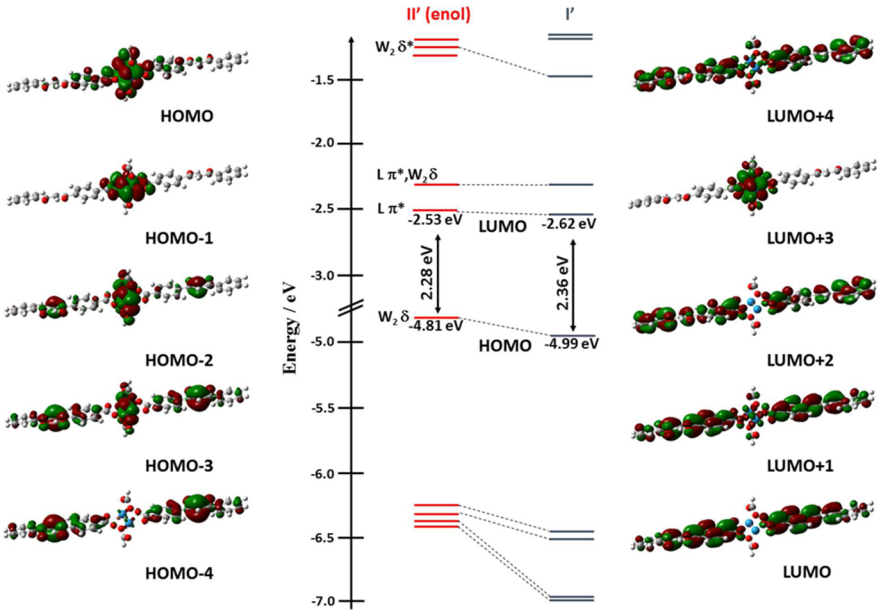

Figure 3. Frontier molecular orbital energy level diagram of model compound **I′** (right) and the enol form of **II′** (left) along with Gaussview 5.0.8 plots of the enol form of **II′** (isovalue = 0.02).

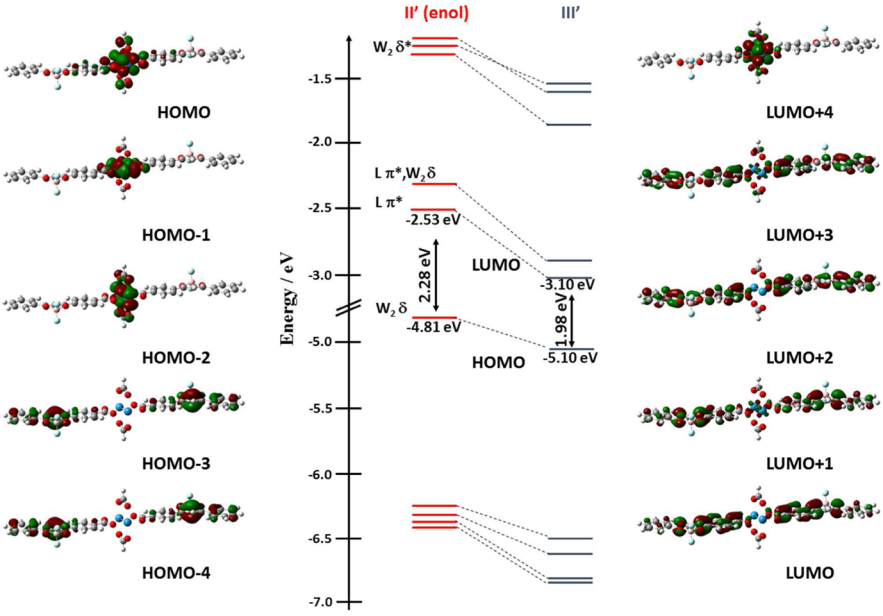

Figure 4. Frontier molecular orbital energy level diagram of the enol form of model compound **II′** (left) and **III′** (right) along with Gaussview 5.0.8 plots of **III′** (isovalue = 0.02).

$[L{-}W_2{-}L]^-$, were used to simulate the ^{1}MLCT excited state and assist in the assignment of vibronic features in the time-resolved infrared spectra.

The frontier molecular orbital calculation for compounds **I′** and **II′** are shown in Figure 3.

For compound **I′** we see that the HOMO is the $W_2\delta$ orbital at ∼−5 eV and the LUMO and LUMO + 1 are the in- and out-of-phase ligand π^* orbitals with the separation of ∼0.3 eV. The LUMO lacks any $W_2\delta$ character, but the LUMO + 1, which is antibonding, is an admixture of $W_2\delta$ and the out-of-phase Lπ^* combination. Below the HOMO lie the $W_2\pi$ molecular orbitals.

For compound **II′** we see a similar set of combinations for the $W_2\delta$ as the HOMO and likewise a set of LUMO and LUMO + 1 with an energy separation of ∼0.3 eV. The LUMO + 2 and LUMO + 4 are essentially identical combinations of out-of- and in-phase ligand π^* orbitals associated with the outermost benzene ring. Also, below the HOMO comes the two $W_2\pi$ MOs, and further below is a pair of ligand based oxygen lone pair orbitals.

For compound **I′**, LUMO + 2 and, for compound **II′**, LUMO + 3 correspond to the $W_2\delta^*$ orbitals. Consequently the fully allowed HOMO → LUMO transition for both is 2.4 eV and is MLCT in character.

For compound **III** a frontier molecular orbital diagram is given in Figure 4.

Here, the HOMO is the $W_2\delta$ orbital and the LUMO and LUMO + 1 are the Lπ^* combinations, separated by 0.2 eV, which is slightly less than in compounds **I′** and **II′**. The smaller

DOI: 10.1021/acs.inorgchem.5b01221
Inorg. Chem. 2015, 54, 9438−9446

separation occurs due to a greater amount of mixing between the $W_2\delta$ orbital and the extended π system of the ligands. There is also an additional set of Lπ* orbitals at higher energy, the LUMO+2 and LUMO+3 orbitals. In compound **III**′ the introduction of the $-BF_2$ unit causes all of the Lπ* orbitals to be considerably stabilized. This also results in a reordering of the molecular orbitals when compared with **II**′; in compound **II**′, the $W_2\delta$* orbital was the LUMO + 3, but in compound **III**′ it is the LUMO + 4.

Also for compound **III**, there are two low energy transitions involving the HOMO → LUMO and the HOMO → LUMO + 2, based on the time-dependent DFT calculations. The HOMO → LUMO and the HOMO → LUMO + 2 transitions are predicted to occur at 714 nm (predicted oscillator strength, $f \sim 1.1$) and 434 nm ($f \sim 0.3$), respectively. There is a predicted band at higher energy, 353 nm ($f \sim 1.0$), which is a combination of the HOMO → LUMO + 2, and HOMO − 3 → LUMO + 1 and HOMO − 4 → LUMO (n → π*) transitions. Thus, the lowest energy transition for this compound is the HOMO → LUMO transition at 714 nm which is ^{1}MLCT in character.

Calculations on the anions are best presented later when we compare time-resolved infrared data.

Electronic and Emission Spectral Features. The compounds **I**, **II**, and **III** all are intensely colored: **I** and **II** are blue, and **III** is a pale yellow-green color in solution. Their spectra recorded at room temperature are collectively shown in Figure 5.

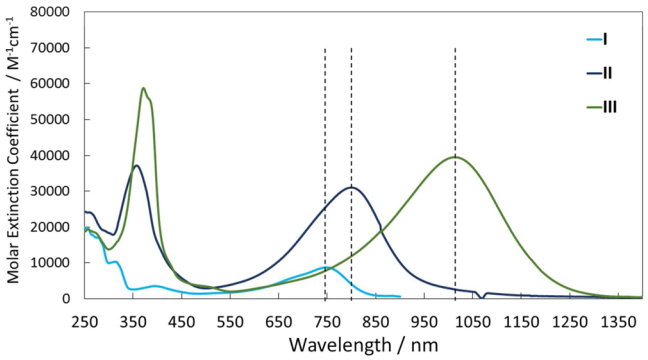

Figure 5. Electronic absorption spectra of compounds **I**, **II**, and **III** in THF at RT. The vertical dashed lines mark the λ_{max}.

Compounds **I** and **II** show rather similar features having an intense absorption at 748 and 796 nm, respectively. Compound **III** shows an intense band at 1017 nm. For compound **I** we also see a band at 400 nm which we can assign to the $W_2\delta$ → $CO_2\pi$* of the T^{i}PB ligands. For the other compounds this band is obscured by both the LL$\pi\pi$* transitions and higher energy MLCT transitions. In the spectra of **III**, the band at 1017 nm represents the HOMO → LUMO transition which is notably red-shifted when compared with the calculated value of 714 nm. This type of calculation employing DFT commonly overestimates the energy of the lowest energy transition in part because they are gas phase calculations and further because of the effects of spin−orbit coupling.

We have also recorded the low temperature and emission spectra of these compounds. The spectra recorded for compound **I** are given in Figure 6.

Here at low temperature we also see the vibronic feature associated with the lower energy transition. For the lowest

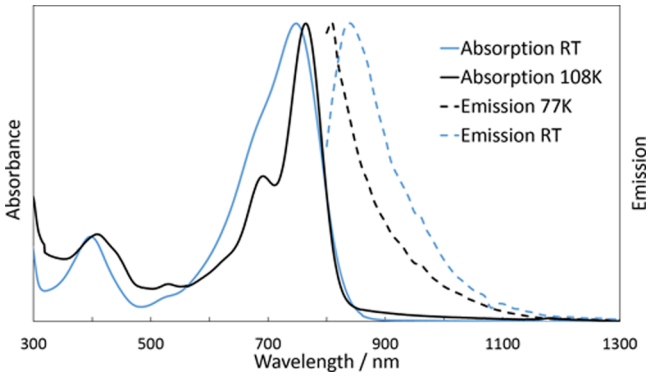

Figure 6. Electronic absorption (at RT and 108 K) and emission spectra (λ_{ex} = 658 nm, at RT and 77 K) of compound **I** in 2-methyltetrahydrofuran.

temperature spectra the absorption and emission peaks move toward each other in energy. At room temperature, the emission spectra is further removed because of variable temperature rotations of the CO_2−aryl plane which upon lowering the temperature favor the structure such as can be seen in Figure 1. We also see the $W_2\delta$ → $CO_2\pi$* transition at 400 nm and the appearance of a weaker but significant transition at 532 nm. This is likely the HOMO → LUMO + 2 as there are no analogous transitions for compounds **II** or **III** in this region.

The spectral data recorded for **II** are similar in effect with temperature (see Figure S7) and for **III** we see a significant red shift of the λ_{max} for the HOMO → LUMO transition from 1017 to 1110 nm upon cooling. This compound has weak fluorescence at 1290 nm (see Figure S8).

Time-Resolved Studies. *Transient Absorption Spectra.* In order to obtain lifetimes, the compounds were all examined by nanosecond, ns, and femtosecond, fs, transient absorption spectroscopy in THF. In general, upon excitation, these W_2 paddlewheel compounds undergo internal conversion within ∼1 ps to populate the S_1, ^{1}MLCT state. These typically have lifetimes ∼1−20 ps before undergoing intersystem crossing to the longer lived ^{3}MLCT state. The ^{3}MLCT states typically have lifetimes of 3−10 ns. A summary of the lifetimes along with kinetic traces is shown in Figure 7.

It is important to note that the precise nature of the kinetic trace is dependent upon which wavelength is selected. The kinetic trace for **I** was taken at a position where there is little ^{3}MLCT absorption, and so the time components consist of internal conversion (τ_1) and the singlet state (τ_2). For **II**, the trace was taken where there is ample ^{3}MLCT absorption, and so a triplet state time component (τ_3) is observed. For **III**, all three components are observed.

The spectra for compound **I**, λ_{ex} = 700 nm, are shown in Figure 8.

There is a ground state bleach at 400 nm due to the $M_2\delta$ to T^{i}PB $CO_2\pi$* absorption, and toward 700 nm where the $M_2\delta$ to Lπ* transition is observed. These, however, are initially somewhat masked by short-lived transient features at 400 and 600 nm. As those absorptions decay with time, the bleaches grow in to give the longer lived triplet spectrum which is typical of this class of compounds. The loss of these positive features occurs within 20 ps which is what we anticipate for the lifetime of the ^{1}MLCT state. Additionally, a fairly intense absorption at 475 nm appears, which increases in intensity ultimately leading to a triplet state absorption at 485 nm. The triplet lifetime is

DOI: 10.1021/acs.inorgchem.5b01221
Inorg. Chem. 2015, 54, 9438−9446

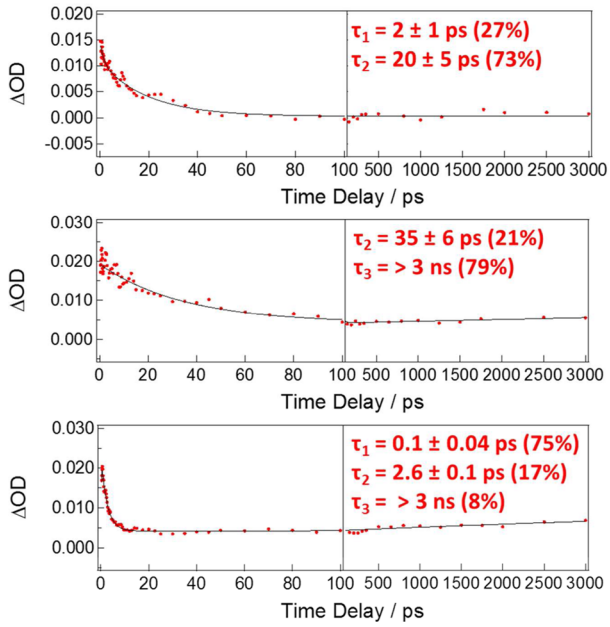

Figure 7. Kinetic traces for the fs TA of **I** (top), **II** (middle), and **III** (bottom) taken at 590, 500, and 470 nm, respectively, where τ_1 = internal conversion time component, τ_2 = singlet state time component, and τ_3 = triplet state time component.

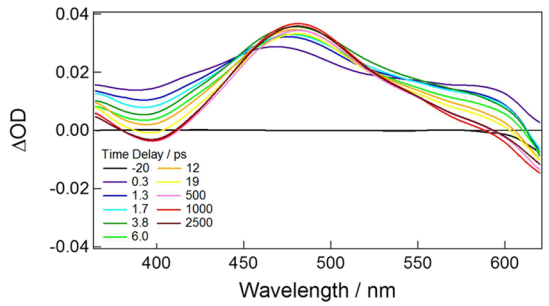

Figure 8. Femtosecond TA spectra of **I** in THF at RT, λ_{ex} = 700 nm.

determined to be between 3 and 10 ns which is typical of a ^{3}MLCT state for these W_2 tetracarboxylate complexes.[8]

The spectra for compound **II** with excitation at 700 nm in THF are shown in Figure 9.

Here we see a bleach at 350 nm due to the ground state $\pi\pi^*$ transition in addition to an initial absorption at 490 nm. With time this decays to the triplet state, and a longer lived absorption at 470 nm persists. The lifetime of this decay process is ∼34 ps which represents the longest lifetime of a

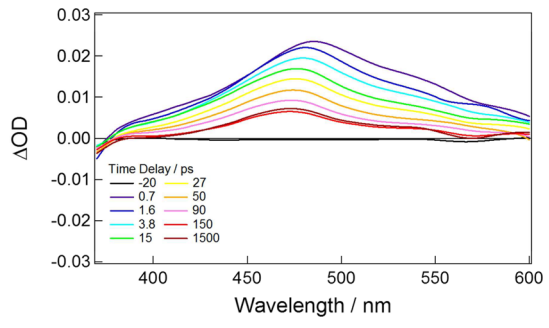

Figure 9. Femtosecond TA spectra of **II** in THF at RT, λ_{ex} = 700 nm.

^{1}MLCT state in these M_2 quadruply bonded complexes.[7] The length of the lifetime presumably arises because of poor mixing of the S_1 and T_n states which are not close in energy. The triplet lifetime is again in the range 3−10 ns.

The spectra for compound **III**, λ_{ex} = 350 nm, in THF are shown in Figure 10.

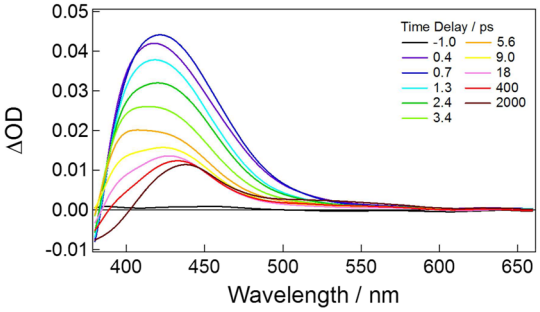

Figure 10. Femtosecond TA spectra of **III** in THF at RT, λ_{ex} = 350 nm.

Here, at early times, there is a ground state bleach of the ^{1}LL$\pi\pi^*$ at around 350 nm and an intense absorption at 425 nm. This absorption quickly undergoes internal conversion from the ^{1}LLCT$\pi\pi^*$ to the ^{1}MLCT with a lifetime of ∼100 fs. This new singlet state decays rapidly to give the triplet state which has an absorption at 440 nm. The lifetime of the ^{1}MLCT is notably shorter, ∼3 ps, which is approximately one tenth of that seen for compound **II**. Also, at lower energy and longer times there is a slight rise of a weak absorption of **III** at 540 nm.

Time-Resolved Infrared Spectra. The ^{1}MLCT and ^{3}MLCT nature of these complexes is uniquely suited to study the progression of the electronic distribution as one state converts to the other by use of time-resolved infrared spectroscopy. The computational methods described earlier for the ground state, anion, and triplet state frequency analysis have been used to aid in the assignment of the vibrational modes. We assume here that the anion calculation represents the case of the ^{1}MLCT state where the complex has been reduced and the charge is delocalized over both ligands. The energies of the bands associated with the anion, however, are anticipated to be somewhat shifted since the calculation neglects the presence of a positive charge on the W_2 center. Due to the limitation of the calculations, including those previously discussed, the ordering of the vibrations is a more important consideration than the precise frequencies. These methods are best employed in identifying principal vibrations, which in addition to the previously published Mo_2 series lead us to the described assignments.[5] A correction factor of 0.96 has been applied to all calculated values discussed in this section (B3LYP, 6-31g*).

The kinetics data for all three compounds is presented in Figure 11 and is in good accordance with the previously discussed fs TA data.

The predicted stretches for all calculations led to some general conclusions which can best be described by grouping similar vibrations together in regions. There were many similarities in the calculated bands for **I**′, **II**′, and **III**′. Each case had relatively high energy stretches which were unique in nature. For **I**′, this was a C═O stretch of the aldehyde whereas in **II**′ and **III**′ these were C—H vinyl stretches. Followed by these intense markers were a series of ring stretches which were either pure ring stretches or ring stretches coupled with the

DOI: 10.1021/acs.inorgchem.5b01221
Inorg. Chem. 2015, 54, 9438−9446

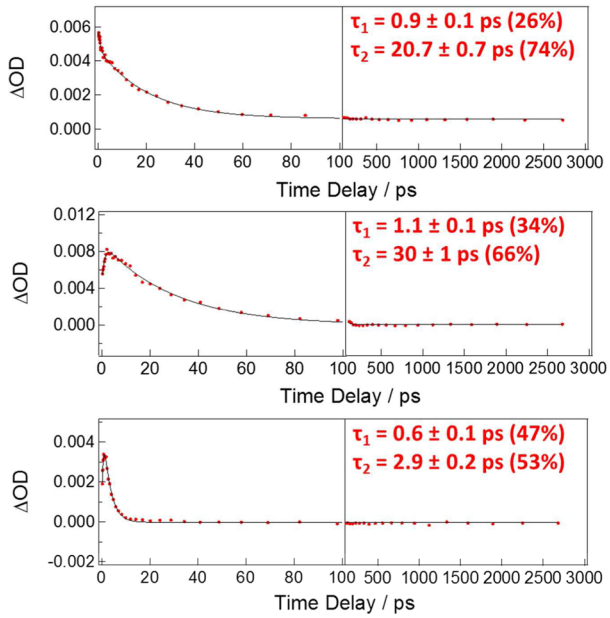

Figure 11. Kinetic traces for the fs TRIR of **I** (top), **II** (middle), and **III** (bottom) taken at 1526, 1640, and 1635 cm^{-1}, respectively, where τ_1 = internal conversion time component and τ_2 = singlet state time component.

high energy modes. In all three cases, the stretch for CO_2 T^{i}PB carboxylates followed the higher energy ring modes. Finally, the lowest energy region in each calculation included bands that were heavily coupled to the CO_2 moiety on the planar aromatic ligands.

We investigated the region 1800−1350 cm^{-1} for compound **I**, with λ_{ex} = 700 nm, shown in Figure 12. The ground state spectrum is depicted by the black dotted line.

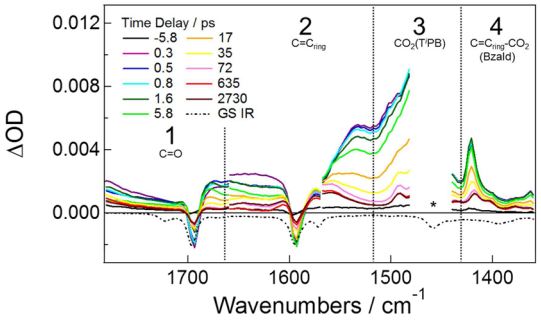

Figure 12. Femtosecond TRIR spectra of **I** in THF at RT, λ_{ex} = 700 nm. The 1490−1450 cm^{-1} gap is due to the THF solvent window, marked by an asterisk.

Upon excitation a ligand based π^* orbital is populated which in general reduces the bond strength and effectively weakens the stretching frequencies associated with the partially reduced ligands. The highest energy band in the frequency analysis for the ground state of **I′** corresponds to the C═C$_{ring}$—C═O stretch. This complements the experimental data in region 1 which features a ground state bleach at 1700 cm^{-1}, and a sharp transient band at 1680 cm^{-1}. The shift to lower energy of the band from the ground state to ^{1}MLCT state indicates more electron density on the aldehyde moiety in the ^{1}MLCT. Region 2 consists of multiple mixed modes of C═C$_{ring}$ stretches. The next band of special note is shown in the ground state spectrum of region 3 at 1470 cm^{-1}, assigned as the $\nu_{as}(CO_2)$ for the T^{i}PB carboxylates. This band and its location are typical for molecules of this type.[5] In the ^{1}MLCT state, this stretch moves to higher energy indicating a removal of electron density from the W_2 core. This is confirmed by the calculations of **I′** and the anion, **I′**$^-$, which predict a shift to higher energy. The decay of the early bands occurs within 20 ps, which is consistent with the fs TA kinetics data. At longer times we see the bands associated with the benzaldehyde ligands indicating that this long lasting triplet state is ^{3}MLCT. The long-lived vibration in region 3 at 1490 cm^{-1} is likely the $\nu(CO_2)$ mode of the T^{i}PB ligands. Notably, there is no intense peak anywhere in region 1 at long times. This implies that there is little extra electron density which resides on the aldehyde unit in the ^{3}MLCT state. This is instructive in determining the electron distribution of the ^{3}MLCT state, since the stretches associated with parts of the molecule further away from the W_2 core show little signal at long times. Further evidence of this comes from the low energy bands that persist for long times in region 4. All bands in region 4 correspond to stretches which exhibit significant coupling of the benzaldehyde-CO_2 moiety with ring stretches. Only those stretches which are close to the W_2 center have significant signal at longer times.These vibrational modes are noted in the Supporting Information in Tables S1 and S2 with comparisons for the neutral compounds, the anions, and the triplet states.

Compound **II** recorded in THF, with λ_{ex} = 700 nm, is shown in Figure 13. Again, the ground state spectrum is shown with the black dotted trace.

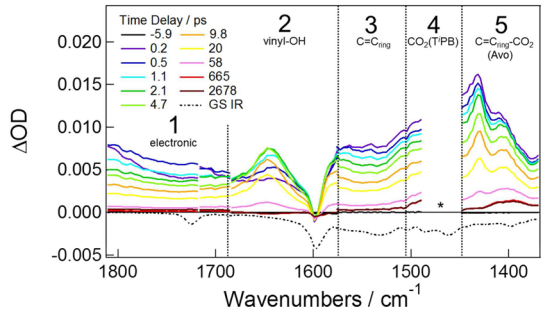

Figure 13. Femtosecond TRIR spectra of **II** in THF at RT, λ_{ex} = 700 nm. The 1490−1450 cm^{-1} gap is due to the THF solvent window, marked by an asterisk.

Here, in region 1, we see no bleach of the ν(C═O) at ∼1720 cm^{-1}. The lack of a strong bleach with the presence of broad bands on top suggests that the excited state of this molecule is in the enol form. A strong and sharp bleach with a related sharp positive feature is expected around this wavelength for the keto form of the ligand. This can be seen in the comparison of the TRIR spectra of the free ligand HAvo and **II** with λ_{ex} = 325 nm in the region 1760−1660 cm^{-1} found in Figures S9 and S10 in the SI where the free ligand exhibits this type of behavior under excitation, but compound **II** does not. The lack of features in this region is in agreement with the previously reported Mo_2 compound where there was also no keto form present (in either the ground or excited states).

In the excited state spectra there is a bleach in region 2 at 1600 cm^{-1} which corresponds to the highest energy band in the calculated ground state of **II′**. This stretch is vinyl/OH in character. Additionally, there is one sharp transient band at

DOI: 10.1021/acs.inorgchem.5b01221
Inorg. Chem. 2015, 54, 9438−9446

~1650 cm^{-1} which decays quickly. This is assigned as the excited state stretch of the ν(vinyl/OH) mode due both to its sharpness and to the associated vibrational calculations of **II**′$^{-}$ of which the highest energy band in the region is of this character. In region 3 there are numerous bands in both the excited and ground states, all of which correspond to ring stretches. Similar to compound **I**, in region 4 of the ground state FTIR of **II** there is a stretch at 1470 cm^{-1} corresponding to the $\nu_{as}(CO_2)$ for the T^{i}PB carboxylates. Again in the ^{1}MLCT this band moves to slightly higher energy, ~1490 cm^{-1}, in a similar manner to compound **I**. All of these ^{1}MLCT bands decay within 30 ps, which is in good accordance with the fs TA data. There is also a broad transition at ~1800 cm^{-1} which may result from a LUMO to LUMO + 1 electronic transition that is formally allowed by the LaPorte selection rule, u → g. The estimated energy of this transition is ~2000 cm^{-1} based off the predicted energies of the molecular orbitals calculated by DFT for the ground state.

There are only two vibrations, at 1490 cm^{-1} and a broad band at 1400 cm^{-1}, that remain at long times and are associated with the triplet state. These appear to be related to the $\nu(CO_2)$ mode of the T^{i}PB ligand and the ν(vinyl-CO_2Avo) mode, respectively. The band in region 4 at 1490 cm^{-1} is similar to the observed stretch in compound **I** and is again indicative of less electron density in the W_2 core at longer times (when compared to that of the ground state). The latter band in region 5 also shifts slightly to lower energy as conversion from the ^{1}MLCT state to the ^{3}MLCT state occurs implying more electron density on the CO_2Avo moiety. Additionally, any bands associated with the outer ring are absent in the triplet state. The strong band at 1650 cm^{-1} (the vinyl stretch) returns to baseline by the later traces which indicate that the extra electron density no longer resides on this part of the molecule. This is supported by relatively intense bands in region 5 that persist at long times. When compared to the predicted triplet stretching modes of **II**′ we find that all of these bands are ring stretches that have significant CO_2 character. This suggests that the electron density is moving toward the vinyl and carboxylate of the Avo ligand and contracting toward the W_2 center in the triplet state. The principal vibrational modes for both the enol and keto forms of **II** are noted in the SI in Tables S3−S6.

The spectra for compound **III**, excited at 350 nm, are shown in Figure 14.

The vibrational modes of compound **III** follow a similar pattern to those of compounds **I** and **II**, but are more complicated due to an increase in the number of vibrational modes in this region. In region 1, an intense transient band

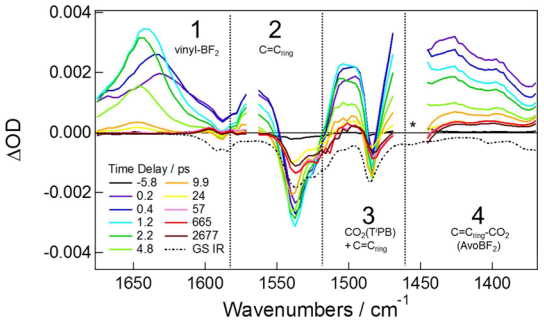

Figure 14. Femtosecond TRIR spectra of **III** in THF at RT, λ_{ex} = 350 nm. The 1490−1450 cm^{-1} gap is due to the THF solvent window marked by an asterisk.

associated with the ^{1}MLCT at 1630 cm^{-1}, likely a combination of ν(C═C_{ring}) modes, grows in to 1650 cm^{-1} and decays back to zero within two nanoseconds. The growth of this peak and its shift to higher energy correspond to ligand planarization. The calculated vibrational modes for **III**′$^{-}$ indicate that the highest energy stretch in this region is associated with the outer rings of the $AvoBF_2$ ligand. In region 2 there is an intense bleach at 1535 cm^{-1}. This stretch is another ring mode which can be tentatively assigned to the ν(C═C_{ring}) of the inner aromatic ring. These assignments were made with comparison to the predicted bands for the ground state of **III**′ which shows several bands in this region of the character previously described. Interestingly, these bleaches initially grow in with time, ~1 ps, corresponding to the alignment of the two aryl ligands with time as they assume a planar position. In region 3, there is an intense bleach which follows the same pattern of growth over the first picosecond. The calculations indicate that this area of the spectrum is expected to have several modes including a T^{i}PB-CO_2 stretch as well as a ring stretch at an almost identical energy. The shift of the bleach to higher energy over 1 ps indicates that there is aryl ligand character in the band at 1485 cm^{-1}. Additionally, in this region we observe two ν(C═C_{ring}) transient bands followed by the THF solvent window at 1470 cm^{-1}. Interestingly, these band are not isolated to the $AvoBF_2$ ligand, but are coupled with the CO_2 of the T^{i}PB ligands in the calculations of **III**′$^{-}$. Finally, in region 4, there are several ν(C═C_{ring}) modes associated with combinations of the rings with contributions from the −CO_2 groups of the $AvoBF_2$ ligands. The calculations of **III**′ indicate that in this molecule (similarly to **I**′ and **II**′) the low energy stretches have significant CO_2 character, while the higher energy bands are the stretches that are not coupled to the CO_2 moieties.

For the triplet state we do not see any band ~1650 cm^{-1} but rather a weak band at 1590 cm^{-1}. This appears to be the highest energy band in this region and is associated with the ν(C═C_{ring}) of the inner ring. At 1500 cm^{-1} there is a band which, when compared to the calculated stretches in this region for **III**′, can be assigned to the vinyl C−H mode. However, the strongest and most notable triplet features come from the lower energy bands in region 4. Here there is a broad signal that remains relatively intense at long time scales. The triplet calculations predict multiple modes in this region, and all of these vibrations are associated with having −CO_2 character. The higher frequencies that are associated with isolated rings are either less intense or simply return to the baseline. At long times, there is no evidence of stretching frequencies associated with the outer ring while concurrently the signals for the CO_2 coupled stretches remain intense. The new distribution of charge in the triplet state appears to only affect the inner and middle rings. Indeed, in comparing the vibrations associated with the ^{1}MLCT and ^{3}MLCT states, a contraction of the charge density toward the central W_2 unit with time is once again observed. These principal modes are compared in Tables S7 and S8 in the Supporting Information.

Concluding Remarks. The preparation of these W_2 quadruply bonded complexes shows much lower energy electronic transitions relative to their Mo_2 counterparts due to the higher energy of the $W_2\delta$ orbital. This is evidenced by the ^{1}MLCT absorption band for compound **III** which falls well into the NIR spectra at 1017 nm. The compounds all show weak singlet emission in the NIR but no emission from the ^{3}MLCT state which has a lifetime in the range 3−10 ns. These states are much shorter than the $^{3}W_2\delta\delta^*$ states which typically

DOI: 10.1021/acs.inorgchem.5b01221
Inorg. Chem. 2015, 54, 9438−9446

have lifetimes on the order of microseconds and exhibit phosphorescence at 800 nm.[8] As expected, the time-resolved spectra show no evidence of an enol−keto transformation in **II** when excited into the ^{1}MLCT or enol $\pi\pi^*$ bands. The unique nature of the W_2 quadruple bond allows for the direct observation of the ^{1}MLCT to ^{3}MLCT conversion. The intersystem crossing is of the right time scale and involves orbitals of the right character for tracking through fs TRIR spectroscopy. We are able to watch the electron density contract on the ligands as the molecule moves from the ^{1}MLCT state to the ^{3}MLCT state.

EXPERIMENTAL SECTION

General Procedures. Due to the air and moisture sensitivity of the new W_2 complexes, compounds **I**, **II**, and **III** were prepared and purified under an inert atmosphere (argon or nitrogen) using standard glovebox and Schlenck line techniques. Throughout the synthesis, purification, and analysis of the compounds, any solvents used were dried and degassed by standard methods. Of special note is that BF_3:Et_2O was used in the making of $AvoBF_2$ and HF is formed as a side product. Additionally high powered lasers were used in the analysis of these molecules which have the potential for both skin and eye damage. 4-Formylbenzoic acid was purchased from Sigma-Aldrich and was used without further purification. The homoleptic starting material, $W_2(T^iPB)_4$, was first prepared according to established procedures.[8] The syntheses of ligands HAvo and $HAvoBF_2$ were reported previously.[5] A 400 MHz Bruker DPX Advance 400 spectrometer was used for all ^{1}H NMR spectra. For all of these spectra the protio impurity in deuterated tetrahydrofuran (THF-d_8) was set at 3.58 ppm. All chemical shifts are given in ppm relative to that value.

Electronic Absorption Spectra. A PerkinElmer Lambda 900 spectrometer was used to record UV−vis−NIR electronic spectra at room temperature using 1 cm × 1 cm quartz cuvettes sealed by Kontes tops with THF as the solvent. The same instrument was used to measure the low temperature UV−vis−NIR electronic spectra using a sealed Specac advanced liquid transmission cell with NaCl windows at 108 K in a glass of 2-methyltetrahydrofuran. This cell was placed inside a Specac variable temperature cell holder with a Specac variable temperature cell controller to regulate and determine the temperature.

FT-IR Spectra. Ground state infrared spectra were recorded with a PerkinElmer Spectrum GX FT-IR spectrometer. Solution samples were sealed in a Perkin-Elmer semidemountable cell with a 4.0 mm CaF_2 front and back window separated by a 0.1 mm Teflon spacer. The spectra were solvent-subtracted and baseline corrected, and then plotted as % transmittance.

Mass Spectrometry. A Bruker ultrafleXtreme mass spectrometer was used to record the high resolution, matrix assisted laser desorption ionization time-of-flight (MALDI-TOF) mass spectrometry data. The instrument was run in positive mode with compounds I, II, and III dispersed in a matrix of dithranol. All of the data collected was standardized with 9 peptides that had molecular weights ranging from approximately 750 to 3100 g/mol. These peptides were supported in a matrix of α-cyano-4-hydroxycinnamic acid (HCCA).

Electronic Structure Calculations. Gaussian09 was used in conjunction with density functional theory (DFT) to optimize the model complexes for each compound in the gas phase.[9,10] For the tungsten atoms, the SDD energy consistent pseudopotentials and the SDD energy consistent basis set were used with the B3LYP functional.[11] For the smaller H, C, B, F, and O atoms, the 6-31G* basis set was used with the same functional.[12,13] In order to ensure the convergence of second derivatives, a force constant analysis was performed on the optimized gas phase structures. Vibrational frequency analysis was then performed to confirm that these structures were global minima on the potential energy surface. A correction factor of 0.96 (B3LYP, 6-31g*) was applied to all calculated vibrations. GaussView 5.0.8 isosurface contour plots are presented in the molecular orbital diagrams with an isovalue of 0.02.[14] The functional and basis sets used for the DFT calculations were used again for the time-dependent DFT (TD-DFT) which allowed for the simulation of electronic absorption spectra.

Time-Resolved Measurements. Ti:sapphire and regenerative amplifier combination (1 kHz, 300 fs fwhm) was employed to record the femtosecond transient absorption[15] spectra as well as the time-resolved infrared[16] spectra. For the fs TA experiments, a sample of each compound was dissolved in THF to give a λ_{max}(MLCT) absorbance of ∼0.3 in a quartz cuvette with a 1.0 mm path length and a Kontes top. The power of the excitation pulses was set to be between 1 and 2 μJ. Wavelength calibrations and group velocity dispersion (GVD) corrections were applied to all spectra. Compounds **I**, **II**, and **III** were excited at 700, 700, and 350 nm, respectively. For the fs TRIR experiment, a sample of each compound was dissolved in THF with an absorbance of ∼0.8 at λ_{max}(MLCT). Solutions were sealed in a PerkinElmer semidemountable cell with a 0.1 mm Teflon spacer between 4 mm CaF_2 windows. The same excitation wavelengths used for the fs TA were again used for the fs TRIR. The excitation power of the laser was set to be between 1 and 1.5 μJ for all compounds. For the ns TA experiment, samples were dissolved in THF to give an absorbance of 0.1−0.3 at λ_{max}(MLCT) in a 1 cm × 1 cm quartz cuvette sealed with a Kontes top. All three compounds were excited at 355 nm with an excitation power of 100 mW.[17]

The resulting kinetics data for the time-resolved experiments were fit to a sum of exponentials, $S(t) = \sum_i A_i \exp(-1/\tau_i) + C$, where A_i is the amplitude, τ_1 is the lifetime, and C is an offset, in Igor Pro 6.0. Standard errors of the exponential fits are given as the error bars of the lifetimes.

Steady-State Emission Spectra. A home-built instrument utilizing a germanium detector was used to collect the steady-state near-IR luminescence spectra. All measurements were recorded in 2-methyltetrahydrofuran using λ_{ex} = 658 nm for compounds **I** and **II**, and λ_{ex} = 405 nm for compound **III**.

Preparation of 4-(3-Oxo-3-phenylpropanoyl)benzoic Acid (HAvo) and 4-(2,2-Difluoro-6-phenyl-2*H*-1λ^3,3,2λ^4-dioxaborinin-4-yl)benzoic Acid ($HAvoBF_2$). These syntheses were reported in previous work.[5]

Preparation of $W_2(T^iPB)_2(Bzald)_2$, I. Toluene (ca. 25 mL) was added to a mixture of $W_2(T^iPB)_4$ (0.180 g, 0.132 mmol) and 4-formylbenzoic acid (HBzald, 0.040 g, 0.266 mmol) resulting instantly in a yellow solution. This was left to stir for 3 days at room temperature in an inert atmosphere box. At the end of 3 days the solution had turned blue. The solution was concentrated by removing toluene under vacuum which was then filtered to capture the solid on a glass frit. The solid was washed with a minimum of toluene, methanol (2 × 10 mL), and hexanes (3 × 20 mL). The compound was dried under vacuum to yield a dark blue powder. ^{1}H NMR (THF-d_8 400 MHz): 10.05 (s, 2H), 8.28 (d, 4H), 8.08 (d, 4H), 6.99 (s, 2H), 2.83 (m, 6H), 1.21 (d, 12H), 0.97 (d, 24H). MALDI-TOF calcd: 1160.29. Found: 1160.37. UV−vis (THF): 748 nm (ε = 9000 M^{-1} cm^{-1}).

Preparation of $W_2(T^iPB)_2(Avo)_2$, II. Toluene (ca. 25 mL) was added to a mixture of $W_2(T^iPB)_4$ (0.188 g, 0.134 mmol) and 4-(3-oxo-3-phenylpropanoyl)benzoic acid (HAvo, 0.0875 g, 0.326 mmol) resulting in the immediate formation of a dark yellow solution. This was left to stir for 3 days at room temperature in an inert atmosphere box which resulted in a deep blue solution. The solution was concentrated by removing toluene under vacuum. The solid was subsequently removed from the solvent by filtering over a glass frit. The solid was then washed with a 10 mL of toluene, 5 × 20 mL methanol, 4 × 30 mL of hexanes. The compound was dried under vacuum to give a blue powder. ^{1}H NMR (THF-d_8 400 MHz): 17.24 (s, 2H), 8.33 (d, 4H), 8.25 (d, 4H), 8.14 (d, 4H), 7.54 (m, 6H), 7.23 (s, 2H), 6.99 (s, 4H), 3.84 (m, 6H), 1.21 (d, 12H), 0.99 (d, 24H). MALDI-TOF calcd: 1396.37. Found: 1396.42. UV−vis (THF): 355, 796 nm (ε = 31 000 M^{-1} cm^{-1}).

Preparation of $W_2(T^iPB)_2(AvoBF_2)_2$, III. Toluene (ca. 15 mL) was added to mixture of $W_2(T^iPB)_4$ (0.236 g, 0.175 mmol) and 4-(2,2-difluoro-6-phenyl-2*H*-1λ^3,3,2λ^4-dioxaborinin-4-yl)benzoic acid ($HAvoBF_2$, 0.110 g, 0.348 mmol) resulting in the eventual formation of a dark green solution. This was left to stir for 3 days at room

DOI: 10.1021/acs.inorgchem.5b01221
Inorg. Chem. 2015, 54, 9438−9446

temperature. The solution was concentrated by removing toluene under vacuum. The solid was removed from the solution by filtering over a glass frit. The solid was then washed with 3 × 25 mL methanol, 3 × 25 mL of toluene, and 5 × 20 mL hexanes. The solid was dried under vacuum to yield a dark green powder. ^{1}H NMR (THF-d_8 400 MHz): 8.50 (d, 4H), 8.30 (t, 8H), 7.70 (m, 4H), 7.63 (t, 4H), 7.00 (s, 4H), 2.84 (m, 6H), 1.21 (d, 12H), 1.00 (d, 24H). MALDI-TOF calculated: 1492.37. Found: 1492.49. UV−vis (THF): 371, 1017 nm (ε = 39 000 M^{-1} cm^{-1}).

■ ASSOCIATED CONTENT

Supporting Information

The Supporting Information is available free of charge on the ACS Publications website at DOI: 10.1021/acs.inorgchem.5b01221.

Characterization, molecular orbital diagrams, electronic absorption and emission spectra for II and III, fs time-resolved infrared spectra, and additional computational information (PDF)

■ AUTHOR INFORMATION

Corresponding Authors

*E-mail: chisholm@chemistry.ohio-state.edu.

*E-mail: gustafson.5@osu.edu.

Notes

The authors declare no competing financial interest.

■ ACKNOWLEDGMENTS

We would like to thank the National Science Foundation for the funding associated with Grants CHE-0957191 and CHE-1266298. We are grateful to the Ohio State University Center for Chemical and Biophysical Dynamics for use of the laser systems, the Ohio Supercomputer Center for computational resources, and Professor Claudia Turro for use of instrumentation. We are also grateful to the CCIC Mass Spectrometry and Proteomics Lab for use of the MALDI, supported by NIH Award Numbers P30 CA016058 and 1 S10 RR025660-01A1. This article is dedicated to Professor Manfred Scheer in honor of his 60th birthday.

■ REFERENCES

(1) Zawadiak, J.; Mrzyczek, M. *Spectrochim. Acta, Part A* **2012**, *96*, 815−819.

(2) Pinto da Silva, L.; Ferreira, P. J. O.; Duarte, D. J. R.; Miranda, M. S.; Esteves da Silva, J. C. G. *J. Phys. Chem. A* **2014**, *118* (8), 1511−1518.

(3) Gaspar, L. R.; Tharmann, J.; Maia Campos, P. M. B. G.; Liebsch, M. *Toxicol. In Vitro* **2013**, *27* (1), 418−425.

(4) Yamaji, M.; Kida, M. *J. Phys. Chem. A* **2013**, *117* (9), 1946−1951.

(5) Chisholm, M. H.; Durr, C. B.; Gustafson, T. L.; Kender, W. T.; Spilker, T. F.; Young, P. J. *J. Am. Chem. Soc.* **2015**, *137*, 5155−5162.

(6) Chisholm, M. H.; Gustafson, T. L.; Turro, C. *Acc. Chem. Res.* **2013**, *46* (2), 529−538.

(7) Chisholm, M. H.; Brown-Xu, S. E.; Spilker, T. F. *Acc. Chem. Res.* **2015**, *48* (3), 877−885.

(8) Alberding, B. G.; Chisholm, M. H.; Chou, Y.-H.; Gallucci, J. C.; Ghosh, Y.; Gustafson, T. L.; Patmore, N. J.; Reed, C. R.; Turro, C. *Inorg. Chem.* **2009**, *48* (10), 4394−4399.

(9) Frisch, M. J.; Trucks, G. W.; Schlegel, H. B.; Scuseria, G. E.; Robb, M. A.; Cheeseman, J. R.; Scalmani, G.; Barone, V.; Mennucci, B.; Petersson, G. A.; Nakatsuji, H.; Caricato, M.; Li, X.; Hratchian, H. P.; Izmaylov, A. F.; Bloino, J.; Zheng, G.; Sonnenberg, J. L.; Hada, M.; Ehara, M.; Toyota, K.; Fukuda, R.; Hasegawa, J.; Ishida, M.; Nakajima, T.; Honda, Y.; Kitao, O.; Nakai, H.; Vreven, T.; Montgomery, J. A., Jr.; Peralta, J. E.; Ogliaro, F.; Bearpark, M.; Heyd, J. J.; Brothers, E.; Kudin, K. N.; Staroverov, V. N.; Kobayashi, R.; Normand, J.; Raghavachari, K.; Rendell, A.; Burant, J. C.; Iyengar, S. S.; Tomasi, J.; Cossi, M.; Rega, N.; Millam, M. J.; Klene, M.; Knox, J. E.; Cross, J. B.; Bakken, V.; Adamo, C.; Jaramillo, J.; Gomperts, R.; Stratmann, R. E.; Yazyev, O.; Austin, A. J.; Cammi, R.; Pomelli, C.; Ochterski, J. W.; Martin, R. L.; Morokuma, K.; Zakrzewski, V. G.; Voth, G. A.; Salvador, P.; Dannenberg, J. J.; Dapprich, S.; Daniels, A. D.; Farkas, Ö.; Foresman, J. B.; Ortiz, J. V.; Cioslowski, J.; Fox, D. J. *Gaussian 09*; Gaussian, Inc.: Wallingford, CT, 2003.

(10) Parr, R. G.; Yang, W. *Density-Functional Theory of Atoms and Molecules*; Oxford University Press: New York, 1989.

(11) Andrae, D.; Häußermann, U.; Dolg, M.; Stoll, H.; Preuß, H. *Theor. Chim. Acta* **1990**, *77* (2), 123−141.

(12) Becke, A. D. *Phys. Rev. A: At., Mol., Opt. Phys.* **1988**, *38* (6), 3098−3100.

(13) Kohn, W.; Sham, L. J. *Phys. Rev.* **1965**, *137* (6A), A1697−A1705.

(14) Dennington, R., II; Keith, T.; Millam, J.; Eppinnett, K.; Hovell, W. L.; Gilliland, R. *GaussView 5.0*; Semichem Inc.: Shawnee Mission, KS, 2003.

(15) Burdzinski, G.; Hackett, J. C.; Wang, J.; Gustafson, T. L.; Hadad, C. M.; Platz, M. S. *J. Am. Chem. Soc.* **2006**, *128* (41), 13402−13411.

(16) Wang, J.; Burdzinski, G.; Kubicki, J.; Platz, M. S. *J. Am. Chem. Soc.* **2008**, *130* (33), 11195−11209.

(17) Byrnes, M. J.; Chisholm, M. H.; Gallucci, J. A.; Liu, Y.; Ramnauth, R.; Turro, C. *J. Am. Chem. Soc.* **2005**, *127* (49), 17343−17352.

DOI: 10.1021/acs.inorgchem.5b01221
Inorg. Chem. 2015, 54, 9438−9446